J Mol Model (2008) 14:581–597
DOI 10.1007/s00894-008-0309-9

ORIGINAL PAPER

Computer molecular models of low-rank coal and char containing inorganic complexes

George Domazetis · Bruce D. James · John Liesegang

Received: 21 January 2008 / Accepted: 1 April 2008 / Published online: 14 May 2008
© Springer-Verlag 2008

Abstract Molecular models of low-rank coal containing water, aqua-ionic species, and transition metal aqua-complexes, were optimised using semi-empirical (SE) quantum mechanics; the model was constructed with properties similar to brown coal; 10–20 wt% water was hydrogen bonded to coal oxygen groups, and the remainder was bulk water. Single point self-consistent field (1scf) computations of coal models provided octahedral mono-, and di-nuclear complexes of Cr, Fe, Co, and Ni, but SE computations often provided distorted structures. Models of char were developed by transforming the coal model containing multi-nuclear metal species into char according to pyrolysis chemistry; the composition of char models containing iron oxides was similar to char samples obtained over 250–800°C. Density functional theory (DFT) optimisation of char models with metal clusters provided low energy configurations of disordered structures with a shallow energy minimum. SE and DFT calculations of char models containing metal clusters were conducted for mechanisms for H_2 and CO formation from pyrolysis and iron-catalysed steam gasification; the active site for gasification was [Fe-C] and its accessibility to H_2O was related to the configuration of the char model. The major steps in iron-catalysed steam gasification were chemi-adsorption of water on [Fe-C], hydrogen abstraction, and oxygen transfer.

Keywords Molecular models · Coal · Char · Metal complexes · Pyrolysis chemistry · Catalytic gasification

G. Domazetis (✉) · B. D. James
Chemistry Department, La Trobe University,
Melbourne, VIC 3086, Australia
e-mail: G.Domazetis@latrobe.edu.au

G. Domazetis
Clean Coal Technology Pty. Ltd.,
Melbourne, Australia

J. Liesegang
Centre for Materials and Surface Science, La Trobe University,
Melbourne, VIC 3086, Australia

Introduction

Coal is used on a large scale as fuel for power generation, resulting in increasing levels of the greenhouse gases that cause climate change. These environmental problems necessitate a reduction in CO_2 emission by improvements in the efficiency of coal usage; such improvements are obtained through a greater understanding of the properties of coal, particularly insights at a molecular level of processes central to coal utilisation, such as, for example, pyrolysis and catalytic steam gasification. Semi-empirical (SE) and ab-initio density functional theory (DFT) calculations are attractive methods for molecular modelling studies, but the main obstacle to such studies in coal stems from the absence of a distinct molecular structure for coal. It is necessary, therefore, to develop a molecular model of coal suitable for high level molecular computations. However, coal is a heterogeneous substance formed from plant remains, comprising lignin, polysaccharides, protein, lipids, resins and pigments, and lesser amounts of other materials, that have been buried and undergone a wide range of chemical transformations over geological time-scale periods [1–3]. The formation of coal via chemical and geochemical processes is termed coalification. The nature of the constituents in coal is related to the degree, or "rank" of coalification. A strategy for developing molecular models of coal must commence with a focus on a particular rank of coal. Rank is generally assessed by a number of methods, including moisture content, volatile

matter, fixed carbon, elemental composition, and distribution of functional groups.

Significant advances in the development of structures for coal have taken place, with impetus from studies related to liquefaction of high-rank coals [4–9]. This approach has often dealt with the extractable portions of the coal substance (often termed the mobile phase) as existing within a non-extractable three-dimensional (3D) macromolecule considered to act as a host for smaller molecular entities. It is uncertain if this concept would be useful in developing a molecular model for low-rank coals. Low-rank coals are perhaps the most heterogeneous of all coals because the mixture of vegetation and forest timber is at a relatively earlier stage of the coalification process compared to that of high rank coals; thus, models of low-rank coals have included those based on samples of decomposing trees found in the coal seam, i.e. these equate to models of modified lignin [10–15]. The great diversity of material and its transformations during coalification for low-rank coal present a formidable challenge to molecular modelling studies. Data from this heterogeneous substance are obtained from well-mixed samples and, consequently, coal molecular models of low-rank coals developed from this data would reflect the average properties of the coal mixture. Low-rank coals contain a relatively large proportion of organic oxygen functional groups that impart hydrophilic properties that retain moisture, and participate in chemical interactions with inorganic species. The coal is mined with a large amount of moisture, of which a relatively small proportion is hydrogen bonded to the coal molecular matrix, and the remainder is 'bulk' water present within the capillaries and macro-pores; e.g. brown coal consists of 60 wt% moisture, including 10–20 wt% hydrogen bonded to the coal functional groups.

The inclusion of inorganic species within the macromolecular matrix of low-rank coal introduces additional complexity, as these would be aqua-species due to the large proportion of water associated with the coal mass. A large proportion of these functional groups are carboxyl and hydroxyl groups, which can act as macro-ligands able to form coordination bonds with aqua mono-, and multi-nuclear hydroxyl transition metal complexes. The functional groups may also participate in pH-dependent aqueous chemistry with ash-forming species such as Na, Ca, Mg, and K. This spans a wide range of chemistry, including that of soluble salts, ion-exchange, mono- and multi-nuclear aqua-metal complexes, and acid-base chemistry [16, 17]; studies at a molecular level should include reaction routes and reaction mechanisms of processes relevant to low-rank coal utilisation, such as pyrolysis and gasification. It is necessary, however, to acknowledge limitations in developing models, and in calculations on molecular models, of low-rank coals, stemming from the restrictions in molecular size imposed by SE and DFT computations.

This paper discusses computer molecular studies of a 3D molecular structure of low-rank coals that models: (1) the elemental composition and distribution of functional groups; (2) behaviour of water, aqua-ionic species, and complexes of the transition metals; (3) the transformations into char, and into char with inorganic species, during pyrolysis; and (4) the chemical reactions routes for H_2 and CO formation during pyrolysis and catalytic steam gasification. These molecular model studies were part of a research program on catalytic steam gasification of low-rank coals to produce hydrogen-rich syngas.

Molecular model and computations

Molecular model of brown coal and char formation

The 3D model of coal was developed by initially constructing a two-dimensional (2D) fragment that incorporated the properties typically measured for brown coal: (1) elemental composition; (2) ratio of aromatic carbon to total carbon, and ratio of aromatic hydrogen to total hydrogen; (3) the distribution of the functional groups as carboxyl, phenolic, methoxyl, carbonyl, hydroxyl and ether; (4) arrangements of aromatic groups—the aromatic groups were connected using aliphatic and ether links; and (5) density of dry brown coal. Aromatic groups were present as either single phenyl, or fused phenyl groups (naphthalenyl); functional groups and linkages were situated at *ortho*- and *para*- positions of phenyl groups. The 3D structure was constructed by connecting the 2D units using hydrocarbon and ether links while maintaining the $C_{(ar)}/C_{(tot)}$ and $H_{(ar)}/H_{(tot)}$ values; the size was restricted to <1,000 atoms by SE computer requirements. Conformational analyses were performed with the Shrödinger MacroModel 9.1 package using the Monte Carlo Multiple Minimum method. Although numerous orientations of a 3D structure were examined, the configuration chosen for our studies was the most stable (as indicated by conformational analysis) because this structure maximised hydrogen bond formation and provided the flexibility for the functional groups to form octahedral and tetrahedral complexes of transition metals. All SE computations were assessed relative to this 3D molecular structure optimised to a ground state. DFT computations, on the other hand, were limited to <300 atoms and thus were restricted to small models of char developed from the coal model.

Molecular models of coal containing aqua-transition metals were developed for divalent metal complexes (Cr, Fe, Co and Ni), and for trivalent metal complexes (Cr and Fe). These species consisted of mono-nuclear and di-nuclear solutions complexes. SE and selected DFT computations were carried out on a number of such structures, and the

results were compared with available crystal structure data for similar molecules [16, 17]. Molecular models of char were developed by removing functional groups from the brown coal model, to mimic the loss of carboxyl, carbonyl, ether and hydroxyl groups observed during pyrolysis. The majority of char models studied contained iron complexes because these have formed the bulk of our studies of catalytic steam gasification, as discussed previously [19–22].

Computation

Small 2D models were assessed using the ACD/Chemsketch package [23]; SE computations were carried out using the PM5 Hamiltonian, with CAChe ab initio 5.04 [24], and initial DFT calculations of transition metal complexes, metal clusters, and small organic molecules were carried out with CAChe 5.04 DGauss 4.1/UC-4.1, using Becke '88; Perdew & Wang '91 theory, with a triple-zeta-valence un-contracted, 63321/531/41 Gaussian basis set (DZVP, A1), and Li-Rn pseudopotential, which includes relativistic effects for heavy atoms. These SE and DFT calculations were carried out to assess structures for use in subsequent, more detailed, SE and DFT calculations.

All final SE computations were carried out with MOPAC2002 [25] at the Australian Partnership for Advanced Computing National Facility, Australian National University, Canberra, Australia (APAC-NF), and DFT calculations were carried out using the Schrödinger Jaguar package [26] at the Victorian Partnership for Advanced Computing facility, Melbourne, Australia (VPAC). The Schrödinger Jaguar computations were at B3LYP theory, exact Hartree-Fock, Slater local exchange functional, Becke's '88 non-local gradient correction, correlation Vosko-Wilk-Nusair local functional and Lee-Yang-Parr local and non-local functional; lacvp** or lacvp3** basis sets, which included effective core potentials (ECPs) for Fe developed at Los Alamos National Laboratory; the basis set was valence-only, containing the highest s and p shells for main group atoms and the highest s, p, and d shells for transition metals including the outermost core orbitals; the 631G basis set was used for atoms not described by ECPs. Polarisation functions on all atoms except for transition metals, and the effective core potentials included one-electron mass-velocity and relativistic corrections. 1scf-DFT calculations were carried out to assess energy changes for specific chemical steps. Geometries were optimised for selected molecular models using DFT-B3LYP and lacvp**; these required large computer resources and were restricted to low accuracy computations.

SE output included: total energy, the heat of formation of the compound from its elements in their standard state (ΔH_f), bond lengths, bond angles, bond orders, atomic partial charges, and contributions of σ and π components to bonds with clusters. All bond lengths and bond angles for our molecular models were compared to available data for similar complexes, particularly transition metal complexes, as discussed previously [16, 17]. ΔH_f is defined in MOPAC as: $\Delta H_f = E_{elect} + E_{nuc} - E_{isol} + E_{atom}$, (where E_{elect} is the electronic energy, E_{nuc} is the nuclear-nuclear repulsion energy, E_{isol} is the energy required to strip all the valence electrons off all the atoms in the system, and E_{atom} is the total heat of atomisation of all the atoms in the system (calculated in eV and converted into kcal mol^{-1} in MOPAC [25]). Wyberg indices in MOPAC provide bond orders that mirror the simple ideas of single, double, and triple bonds; bond orders of less than 0.2 are indicative of "no bond"; the bonds matrix is split into σ–π–δ components, and the net charges, or atomic partial charge, on each atom from MOPAC were the Coulson charge, while for specific models Mulliken populations and atomic partial charges were also computed.

DFT and 1scf-DFT data included total energy for each structure (Hartrees), bond lengths and angles, and Mulliken atomic partial charges; DFT optimised geometries were provided at each optimisation step, and a plot of the energy change for each step, relative to the starting structure, generated an energy profile that identified the lowest energy molecular structure.

Calculations were carried out using smaller molecules to obtain energy barriers and transition states for reaction mechanisms similar to those examined for the complicated char reaction systems, and these have been previously discussed [20–22]. Results obtained for a simple system consisting of a graphitic structure containing the C≡ C group reacting with FeO (and Fe_2O), gave similar relative changes in energies for the sequence leading to CO formation, from 1scf-SE and 1scf-DFT calculations [21].

SE molecular modelling computations of a coal molecule containing large amounts of water were too large for SE computations, and could be optimised only using the MOZYME routine in MOPAC [25]; MOZYME uses localised molecular orbitals for closed shell systems, and thus requires lower memory and computer walltime. A full SE treatment of structures containing transition metal complexes requires multi-electron configuration interactions (MECI); such calculations for the molecular model of coal required excessive computer wall-time, and only 1scf-PM5 calculations could be carried out using MECI for micro-states resulting from single electron excitations. 1scf computations were also carried out for chars with metal clusters, and these were used to obtain differences in the calculated energies for two identical molecular models that had undergone one internal change. While 1scf treatment of chars with metal clusters was relatively straightforward, SE results provided structures with short distance between the transition metal and adjacent hydrogen atoms, and each such

optimised structure was examined to assess the extent of metal–atom interactions. This approach proved useful for studies of pyrolysis and steam gasification chemistry; the various reaction routes for pyrolysis chemistry were assessed using all data provided by 1scf-PM5, 1scf-DFT, and SE calculations.

It should be noted that a number of models were of chemically reactive systems at elevated temperatures; SE optimisation would normally provide the ground state, and such computations subsequently often proved difficult to complete. While SE calculations could be carried out by relaxing the default conditions for geometry optimisation, removing safety checks resulted in catastrophic failure. SE calculations for difficult structures were performed by varying the minimum allowed ratio for energy change in MOPAC; in minimum energy searches it is usually desirable that the energy decreases in each iteration, and MOPAC searches for lower energy changes for rigid systems by stipulating values for a maximum and minimum allowed ratio for energy change. Calculations were also terminated in some cases at the default value of the trust radius in MOPAC; in cases where the optimisation terminated before the stationary point had been reached, the trust radius was set to a lower value, or to zero, to allow the program to continue searching for a ground state.

Results

Coal molecular model, water, and ionic species

The molecular model was developed to reflect typical experimental data for brown coal, as shown in Table 1. The distribution of oxygen groups measured by conventional chemical analyses identified only between 54 wt% and 64 wt% of the total oxygen, leaving 34 wt% to 46 wt% unaccounted for [27, 28]; consequently the experimental data for oxygen groups in Table 1 has been supplemented by our XPS data for the surface composition of brown coals, which provided the organic oxygen in brown coals as 23% carboxyl, 18% carbonyl, and the remaining 59% distributed amongst phenol, hydroxyl, ether and methoxyl groups, as discussed previously [27].

The molecular model of coal, and the model containing various amounts of water, were all optimised to the ground state; the increased stability with water, as indicated by heats of formation, was −56.9±2.8 kcal per H_2O. Data for these coal models with the water molecules situated within the coal structure, and with the same number of water molecules at a distance as water vapour, gave a difference of +4.6 kcal/H_2O for water as vapour outside the coal molecule.

MOPAC provided the dimensions of the molecule [25], which were used to calculate a molecular volume; this was used to obtain changes in the volume of the molecular structure with the addition of water. The molecular volume did not change appreciably with the addition of water as long as the water molecules were within the molecular model, as observed for up to ~20 wt% water. Increasing amounts of water were situated on the outside of the coal structure until the coal molecular model was enveloped by liquid water. Larger amounts of water required at least two coal structures, with excess water situated in the space between the two coal molecules. SE-MOZYME calculations performed for a model consisting of two coal structures and 53 wt% water yielded a volume that had increased by a factor of ~1.8 per coal molecule and, consequently, a decrease in density; this is consistent with the lower density of as-mined brown coal compared to that of dry coal [29]. A model of at least four coal molecules and water distributed within the coal structures was required for ~60 wt% water, which was too large for SE

Table 1 Properties of the molecular model compared with those typical of brown coal

Molecular model data	
Composition	C_{258} H_{256} N_2 O_{78} S
Molecular weight	4,664.887
Analysis	C 66.4%; H 5.5%; O 26.8%; N 0.6%; S 0.7%
$C_{(ar)}/C_{(tot)}$	0.6; (O/C) atomic ratio 0.3
$H_{(ar)}/H_{(tot)}$	0.2; (H/C) atomic ratio 1.0
Oxygen groups	$O_{(COOH)}$ 21%; $O_{(Ph\text{-}OH)}$ 34%; $O_{(O\text{-}CH3),\ (C\text{-}O\text{-}C),\ (C\text{-}OH)}$ 25%; $O_{(C=O)}$ 11%; other=9%
Experimental data for brown coal [18]	
Analysis	C 67.8%; H 4.9%; O 26.4%; N 0.3–0.6%; S 0.3 to 0.6%
$C_{(ar)}/C_{(tot)}$	0.57–0.65; (O/C) atomic ratio ~0.3
$H_{(ar)}/H_{(tot)}$	~0.3; (H/C) atomic ratio ~0.9
Oxygen groups	$O_{(COOH)}$ 17–23%; $O_{(Ph\text{-}OH)}$ 35–38%; $O_{(O\text{-}CH3)}$ ~12%; $O_{(R\text{-}OH)}$ ~4%; $O_{(RC=O)}$ ~23%

computations, and thus was optimised using molecular mechanics.

The relative changes in the energy of a molecular model that could be attributed to a particular ionic species in the coal, and data of atomic partial charges on ionic species (carboxylate and Na^+ or Ca^{2+}), were obtained. This data was obtained using a coal structure containing a simple anion-cation unit, with a given number of water molecules within, and outside, the coal, and with a hydration sphere for the inorganic species. A model containing a sodium cation and ionic sodium chloride was also optimised to mimic mined brown coal containing chloride. The ΔH_f values for the coal containing sodium at a distance, and within, the coal molecule show that the molecule containing the cation was energetically favoured (with the same number of water molecules). Similar calculations for coal with the calcium cation and two carboxylate anions indicated the structure was less energetically favoured compared to the coal model with the same number of water molecules. However, larger molecular models consisting of two coal molecules, water, and the calcium placed in the space between the two coal molecules, indicated that this configuration with calcium was energetically favoured.

Low-rank coal containing transition metal complexes

Table 2 contains 1scf-PM5 and SE calculated values of ΔH_f, total energy, atomic partial charges on the metal centre, and bond lengths to the metal centre, for coal

Table 2 Molecular models of aqua-transition metal complexes in coal

Transition metal in the coal molecular model	ΔH_f (kcal)	Total energy (eV)	Partial charge $M^{\delta+}$	Wt% metal	M-O Å	M←O Å
1scf-PM5						
Cr^{2+} ($43H_2O$)	−4,969.8	−70,487.3	0.0	0.95	1.94	2.15
Fe^{2+} ($43H_2O$)	−4,941.7	−70,708.5	0.7	1.02	1.93	2.14
Co^{2+} ($43H_2O$)	−5,175.8	− 70,803.7	0.9	1.07	1.91	2.13
Ni^{2+} ($43H_2O$)	−5,010.3	−70,849.7	0.2	1.07	1.90	2.12
$[FeOH]^{2+}$ ($42H_2O$)	−4,957.8	−70,695.9	1.0	1.02	1.92	2.14
Cr^{3+} ($43H_2O$)	−4,956.0	−70,474.6	0.4	0.95	1.93	2.16
Fe^{3+} ($43H_2O$)	−4,944.6	−70,690.6	0.8	1.02	1.92	2.14
$[Cr_2(OH)_2(4H_2O)]^{2+}$	−2,881.4	−59,358.4	−0.2, −0.3	2.13	1.88	2.15
$[Fe_2(OH)_2(4H_2O)]^{2+}$	−2,860.0	−59,790.8	0.5, 0.5	2.29	1.89	2.15
$[Co_2(OH)_2(4H_2O)]^{2+}$	−3,359.1	−59,991.8	1.0, 0.9	2.41	1.91	2.14
$[Ni_2(OH)_2(4H_2O)]^{2+}$	−3,043.2	−60,084.3	0.2, 0.2	2.40	1.86	2.12
$[Cr_2(OH)_2(4H_2O)]^{4+}$	−2,736.9	−59,325.6	0.4, 0	2.14	1.90	2.17[a]
$[Fe_2(OH)_4(3H_2O)]^{2+}$	−2,967.7	−60,080.8	1.1, 0.7	2.28	1.93	2.14
$[Fe_2(OH)_2(2H_2O)]^{4+}$	−2,748.4	−59,163.2	1.0, 1.0	2.31	1.92	2.14
$\{[Fe_2(OH)_n]^{(6-n)}$ $[Fe_3(OH)_m]^{(9-m)}\}$	−2,933.5	−62,671.2	1.0,0.6,1.0,0.5,0.8	3.26	1.89 1.92	2.17 2.15
$\{[Fe_4(OH)_7(H_2O)_3]^{5+}$ $[Fe_3(OH)_4]^{5+}$, $23H_2O\}$	−4,229.7	−71,052.2	1,1,0.8,1.1, 1.1,1.0,1.0	6.86	1.92 1.93	2.20 2.27
SE-PM5						
Cr^{2+} ($43H_2O$)	−5,558.9	−70,514.0	−0.6	0.95	1.93	1.99
Fe^{2+} ($43H_2O$)	−5,543.8	−70,729.9	0.6	1.02	2.06	2.11
Fe^{3+} ($43H_2O$)	−5,597.5	−70,719.0	0.8	1.02	1.99	2.05
Ni^{2+} ($43H_2O$)	−5,705.7	−70,879.8	0.2	1.07	1.82[b]	2.16[c]
$[Cr_2(OH)_2(3H_2O)]^{4+}$	−3,357.7	−59,352.5	0.3, −0.2	2.14	1.98	2.11[d]
$[Fe_2(OH)_2(4H_2O)]^{2+}$	−3,298.8	−59,809.7	0.5, 0.5	2.29	1.92	2.13
$[Co_2(OH)_2(4H_2O)]^{2+}$	−3,850.2	−60,013.1	1.0, 1.0	2.41	1.92	1.98
$[Ni_2(OH)_2(4H_2O)]^{2+}$	−3,727.4	−60,114.0	−0.7, −0.1	2.40	1.87[e]	2.25[e]
$[Fe_2(OH)_4(2H_2O)]^{2+}$	−3,345.3	−59,785.1	1 .0, 0.5	2.29	1.98	2.18
$[Fe_2(OH)_4(7H_2O)]^{2+}$	−3,236.2	−61,293.7	1.0, 0.6	2.25	1.92	2.16

[a] Structure distorted by H_2O at 2.9 Å from Cr
[b] Distorted structure with bidentate ligand (C=O)→Ni at 2.50 Å
[c] Distorted structure with additional coordination bond OH→Ni at 2.36 Å
[d] Distorted structure with close H···Cr distance
[e] Distorted structure with additional coordination bonds H_2O→ Ni, bidentate carboxylate ligand and closer H_2O···Ni at 2.35Å and OH···Ni at 2.45 Å

models containing mono-nuclear and di-nuclear transition metal complexes. The molecular models of coal with a total of 43 water molecules contain octahedral transition metal complex $[M(H_2O)_3]^{2+}$ where M=(Cr^{2+}, Fe^{2+}, Co^{2+}, Ni^{2+}), $[Cr(H_2O)_3]^{3+}$, $[Fe(H_2O)_3]^{3+}$, and $Fe(OH)(H_2O)_3]^{2+}$; these form bonds with coal carboxyl groups, coordination bonds to water molecules, and a coordination bond with a hydroxyl group in coal. The identical molecular configuration was used in each computation, with the same functional groups bonded to the metal centres, but with the identity of the transition metal changed. Some metal complexes were optimised to a ground state with a distorted octahedral structure; in these, the carboxyl groups acted as bidentate ligands, and also contained a short O–H···H–O–H distance between the hydroxyl group coordinated to the metal centre and a water molecule (indicative of an acidic proton as $[H_3O]^+$). Coal models containing di-nuclear metal complexes, $[M_2(OH)_2(4H_2O)]^{2+}$, were examined, where M=Cr (II), Fe(II), Co(II), Ni(II), and also $[M_2(OH)_2(4H_2O)]^{4+}$ where M=Cr(III) and Fe(III). The SE-optimised coal structure containing the Ni complex was distorted, with water and hydroxyl groups situated at shorter distances.

Char formation and pyrolysis chemistry

Molecular models of char were developed by removing functional groups from the coal molecular model to mimic pyrolysis chemistry, as previously discussed [20, 21]. At low temperatures, the coal model lost carboxyl groups as CO_2 and CO at given molar ratios; this provided a wt% loss and CO_2:CO ratio similar to that obtained experimentally for brown coal (on a dry ash free basis). ΔH_f values of the ground states, the weight loss, and the composition of the char models are listed in Table 3, and are labelled as: Char1 to Char3 for chars formed at 200–400 °C, Char4 at ~400 °C, Char 5 at 500–600 °C and Char6 at 700–800 °C. Direct comparison between the relative weight loss of models with brown coal was complicated by the variations in experimentally measured weight loss and CO_2:CO ratios with changes in the rates of heating; the data in Table 3 are typical for brown coal subjected to relatively low heating rates to the specified temperatures [20]. For example, the elemental composition, weight loss and gases ratio for Char1 (C 69.8%, H 5.6%, O 24.3%; weight loss 11.7 wt%, and a CO_2:CO ratio of 2.8), was similar to char obtained from brown coal at ~300 °C (C 70.1%, H 4.1%, O 25.4%; weight loss 14 wt%, and a CO_2:CO ratio of 2.8). The formation of Char6 required the loss of all carboxyl, carbonyl, ether, and ~40% of phenolic groups; the weight loss for this model was similar to the experimental weight loss for brown coal at 700–800 °C. While the weight loss was due mainly to decomposition of oxygen groups, loss of small hydrocarbons also took place, and consequently hydrocarbon entities were removed to maintain the required carbon and hydrogen content; this included loss of alkane groups and alkane or carbonyl groups that linked the 3D structure. Hydrogen loss was accompanied by the formation [C=C] double bonds; the loss of groups that acted as links resulted in a char model consisting of two or three large fragments, forming a disordered or 'entangled' 3D arrangement. All of the char molecular models were optimised to a ground state.

Molecular models of char with iron oxides reflected: (1) the weight losses observed experimentally for brown coal containing iron species, (2) the iron oxide phases measured with XRD, and (3) the at%Fe and at%O data obtained using XPS. For example, the model of char with Fe_3O_4 consisting of octahedral Fe(III) and tetrahedral Fe(II) centres, was developed from a coal model containing $[Fe_3(OH)_n]^{(9-n)+}$ complexes. The pyrolysis chemistry at higher temperatures included reduced metal species in char; this was modelled using char containing $[M_3O_2]$, $[M_3O]$ and $[M_3]$ clusters (M=Cr, Fe, Co, Ni). The relationship between iron oxides and iron clusters postulated in these models, and the distribution of multi-nuclear aqua-hydroxyl species added to brown coal, which act as precursors for the species in char, has been discussed [21, 22].

The 1scf treatment of char models containing metal oxides and metal clusters, provided structures with typical bond lengths. SE optimisation for these various char models, however, always provided structures containing short [M···H] and [M···C] distances; examination of a large

Table 3 Models of char formed from the coal molecular model

Model	SE ΔH_f (kcal)	Weight loss (%)		Composition of model (%)			
		Model	Measured	C	H	O	N
Char1	−2,299.0	1 1.7	14	69.8	5.6	24.3	0.3
Char2	−1,810.5	1 3.8		72.0	6.2	21.1	0.7
Char3	−1,813.5	1 5.8	15	71.6	6.1	21.6	0.7
Char4	−1,228.6	2 1.8	30	73.1	5.0	21.1	0.8
Char5	−278.9	4 4.6	50	82.7	6.3	10.5	0.5
Char6	41.4	56.8	54	85.7	5.6	7.9	0.7

number of these structures indicated that energetically favoured structures were obtained by hydrogen abstraction from nearby [OH] and [CH] groups. The data in Table 4 summarises the results of SE optimised structures of chars with various transition metal species.

1scf-DFT calculations were carried out for Char6 and the [Char6(M_3O_n)], with the clusters Cr_3O, Fe_3O_2, Fe_3O, Fe_3, Co_3O_2, Co_3O, Co_3, and Ni_3; DFT geometry optimisation was performed on a number of models of Char6 and Char6 containing Fe and Co clusters. DFT geometry optimisation on models of Char6 containing the [Fe_3] or [Co_3] cluster, was done by forming coordination bonds with hydroxyl groups [M ←OH], and by removing H_2 from two hydroxyl groups, to form [M–O–C] bonds between the metal centres and oxygen groups. The energy change at each step of the geometry optimisation was used to obtain the energy profiles for the structures, as shown in Fig. 1; this profile is typical for all of the Char6 models. The lowest energy structures reflect changes in the positions of the individual char groups, and the configuration of char fragments relative to the metal cluster.

The bond lengths for the lowest energy structure obtained using DFT geometry optimisation are listed in Table 5; bond lengths have been compared to those reported from DFT calculations of various single clusters of Fe, Ni and Co, and our own results for these clusters. Bond lengths [M–M] for small clusters range from 1.9 Å to 2.4 Å [30–38]; the metal–metal and metal–oxygen bond lengths from our DFT-optimised char molecule often differed from those obtained for the comparable single cluster molecule. Figure 2 represents the DFT geometry optimisation for the lowest energy structures for Char6 and [Char6(Co_3)]. While the results for Char6 yielded a minimum energy, these calculations for char containing metal clusters show a broad minimum, in which a small change in energy was observed for each step. Inspection of each of these structures revealed that the small changes in the energy minima were due to changes in the orientation of the char groups relative to the cluster. DFT optimisation was also carried out for structures formed after loss of H_2 and CO during pyrolysis; such structures contained [M–C] bonds.

Table 4 Optimized semi-empirical (SE) char models

Model	ΔH_f (kcal)	Wt% metal	Bond lengths (Å)[a]				
			M-M		M-O		M←OH
Char1 (Fe_3O_4)	−2,124.7	3.7	2.86	2.82	1.77	2.04	2.07, 2.22
Char1 (Fe_3O_2)	−2,133.8	3.7	1.77	2.68	1.76	2.03	2.15[b]
Char1 (Fe_6O_8)[c]	−2,366.2	7.1	3.02	3.32	1.86	1.98	2.14, 2.28
Char5 (Fe_5O_5)	−252.7	5.7	2.77	3.09	1.90	1.94	2.16, 2.20
Char6 (Fe_3O_2)[d]	79.1	7.6	2.88	2.92	1.98	2.06	2.17
Char6 (Fe_3O_2)[e]	408.8	7.6	2.26	2.83	1.93	1.94	2.19
Char6 (Cr_3O_2)1scf	315.0	7.1	2.78	2.77	1.88	1.93	2.18
Char6 (Co_3O_2)1scf	5.2	7.9	2.73	2.75	1.86	2.12	2.16
Char6 (Ni_3O_2)[f]	−316.2	7.0	2.73	3.07	1.75	1.78	2.15
Char6 (Cr_3O)	176.5	7.1	3.92	3.38	1.64	1.65	2.93
Char6 (Co_3O)	−355.2	8.0	3.93	3.37	1.58	1.65	1.78
Char6 (Fe_3O)1scf	532.3	7.6	2.52	2.51	1.90	2.07	2.16
Char6 (Fe_3O)[g]	65.2	7.6	1.78	2.15, 2.72	1.91	1.98	–
Char6 (Ni_3O)[h]	−251.8	8.0	2.82	2.61	1.80	1.81	2.39
Char6 (Cr_3)[i]	197.1	7.2	2.23	2.77	–	–	2.14
Char6 (Fe_3)[j]	131.3	7.7	1.78	2.19	–	–	2.30
Char6 (Co_3)	−383.5	8.1	3.52	4.63	1.69	2.68	–[k]
Char6 (Ni_3)[l]	−263.0	8.0	2.60	3.15	–	–	2.06

[a] These values of bond lengths are typical and are not a complete listing
[b] Distorted with Fe ←OH bonds at 2.5 Å to 2.7 Å
[c] Fe_6O_8 with short Fe···H distances 2.0 Å, 1.82 Å, H occupied vacant Fe sites
[d] Fe-H bonds 1.53 Å and Fe-C bonds 1.93 Å
[e] Contained Fe-H 1.81 Å, and Fe-C 2.24 Å
[f] Ground state contained Ni···(Ph) π bonding at 2.45 Å, to 2.30 Å
[g] Bonds Fe-H 1.90 Å, Fe-C 2.02 Å
[h] Ni···(ph) π bonding at 2.15 Å to 1.85 Å
[i] Cr-H bonds 1.41Å, and Cr-C bonds 2.06 Å
[j] H abstraction, formed Fe-H 1.58 Å, Fe-C 1.95 Å
[k] H abstraction, formed Co-H at1.39 Å. Co-C at 2.15 Å
[l] Ni-Ph π bonds at 2.3 Å to 2.5 Å

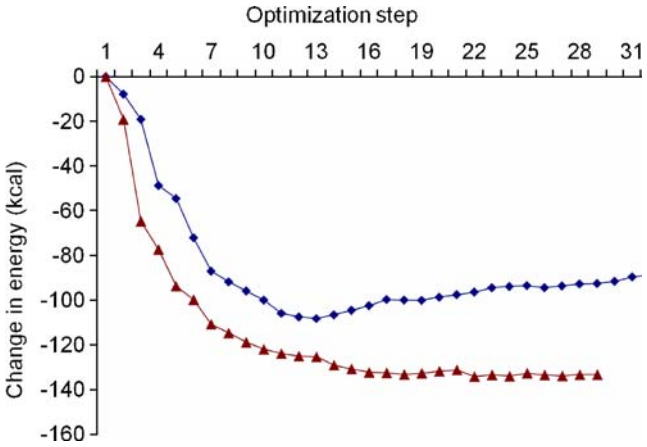

Fig. 1 DFT geometry optimisation of [Char6] (♦) and [Char6(Co_3)] (▲)

The energy minimum observed for the char model in Fig. 1 is for the structure shown in Fig. 2a, which contains entangled fragments; the subsequent steps in the DFT computations provide higher energy structures and, in these, the fragments are separated until the higher energy configuration consists of three distinct organic molecules or fragments. This result shows that the entangled char fragments provide the lowest energy configuration for the char model, and is consistent with the nature of char obtained from low-rank coals, which is non-graphitic, or disordered char. The configuration changes to a lower energy were also observed for the char model with the metal cluster, but the subsequent changes to a higher energy 'untangled configuration' observed for the char molecular model, were not observed for the char with the cluster. This was because the cluster had formed bonds with oxygen groups on the different fragments, and bound the char fragments together. The char-cluster molecule was optimised to the structure shown in Fig. 2b, and further geometry optimisations provide a similar structure with the same energy, as indicated in Fig. 1.

1scf-DFT calculations were used to examine structures involved in various reaction routes to H_2 and CO formation; these provided energy changes for molecular models describing a mechanism of H_2 and CO formation for char molecules containing metal species, and for catalysed gasification of water. The reaction routes for these processes have been discussed [20–22]. An example of this modelling effort is the sequential modelling of [Char6(Ni_3)]; Fig. 3a–c are three of the structures used in the studies of hydrogen abstraction and formation; Fig. 4 is a graph of the changes in the heat of formation obtained for [Char6(Ni_3)], based on a mechanism consisting of a sequence of six internal changes to the molecule, ultimately leading to the formation and loss of H_2. The bond lengths for these structures are: Fig. 3a: Ni–Ni 2.306 Å, 2.296 Å, 2.297 Å; Ni ←OH 2.146 Å, 2.148 Å, 2.138 Å; Fig. 3b: Ni–Ni 2.308 Å, 2.303 Å, 2.296 Å, Ni–O 1.893 Å, 1.887 Å, Ni ←OH, 2.140 Å; Ni–H 1.480 Å, 1.487 Å. Ni–Ni bond lengths reported for DFT computations of the Ni_3 cluster are: 2.283 Å (2.230 Å), and 2.250 Å (2.220 Å); Ni–H and Ni–CH species have been reported to form from the reactions between nickel clusters and methane [30, 31].

Catalytic steam gasification yielding H_2 and CO

A number of reaction sequences were examined using 1scf-SE and 1scf-DFT calculations to develop a mechanism for catalytic gasification with steam yielding H_2 and CO. The mechanism for the loss of H_2 and CO from [Char6(Fe_3)] during pyrolysis included abstraction of H from nearby [O–H] and [C–H] groups (shown to be the most energetically favoured route), and elimination of CO from [Fe–O–C] (less energetically favoured route) to give [Fe–C]; this

Table 5 Bond lengths of lowest energy density functional theory (DFT) geometry for Char6 with metal clusters

Cluster	Bond lengths (Å)								
	M-M	M-M	M-M	M-O	M-O	M←OH	Typical C-O		
Fe_3[a]	2.285	2.305	2.293	–	–	2.145, 2.162	1.368	1.364	1.404
Fe_3[a]	2.194	2.165	2.235	–	–	2.045, 2.105	1.390	1.369	1.397
Fe_3[b]	2.347	2.158	2.242	1.868	2.018	2.032	1.373	1.370	1.403
Co_3	2.327	2.261	2.256	1.848	1.782	1.913	1.344	1.365	1.339
Co_3[c]	2.275	2.117	2.263	–	–	2.111, 2.202	1.390	1.088	1.367
Fe_3O_2[d]	2.411	2.601	2.531	1.821	1.928	2.153	1.358	1.404	1.382

[a] Two configurations of {Char6[Fe_3]} were examined
[b] Model after loss of CO, Fe-C bond length 1.847 Å
[c] The cluster contains coordination bonds only
[d] Structure after loss of CO and H_2, Fe-C bond lengths 1.939 Å, 1.923 Å, in Fig. 5a; Fe-C bond lengths for small clusters reproted at 1.61 Å to 1.93 Å [34]; Fe-Fe bond lengths erported at 2.14 Å for Fe_3 clusters [35]; Fe-O bond lengths reported for small FeOn clusters 1.577 Å to 1.839 Å [36]

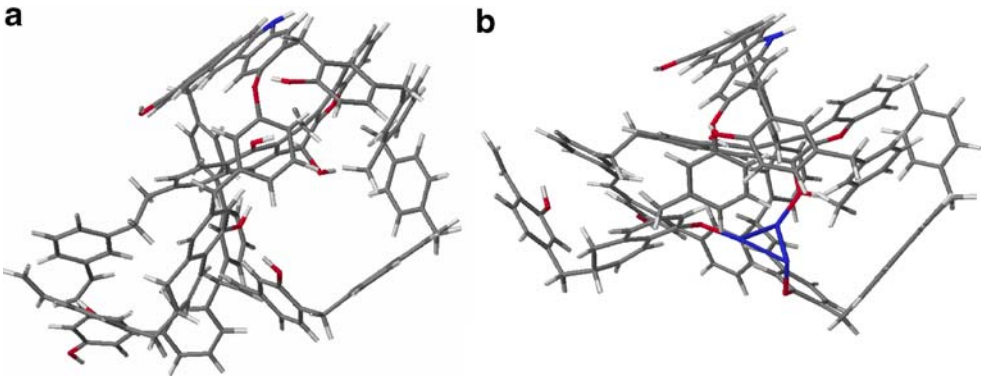

Fig. 2a,b Density functional theory (DFT)-optimised structures. **a** CharD5A, **b** CharD5A (Co_3). *Blue* Co

group has been identified as the active site for reaction with H_2O. The basis for identifying [Fe–C] as the active site for catalytic steam gasification was that this provided the largest change in energy on forming the [H_2O →Fe–C] group, and also the regeneration of the [Fe–C] site occurred after loss of CO. The geometry of a structure containing [Fe–C] bonds, optimised using DFT, is shown in Fig. 5a and the energy change with each step in the optimisation shown in Fig. 5b.

Modelling computations were performed to assess the energy changes when H_2O formed coordination bonds to [M–O], [M ←OH] and [M–C] groups (M = Cr, Fe, Co and Ni) within char; the majority of these models contained iron clusters and thus most of the data deal with the [Fe–C] group. These studies required a number of char molecular models with various orientations of the [Fe–C] sites within a larger molecular environment. Such molecular models consisted of an ensemble of char molecular models of the type {x[Char6(Fe_3)]}, {x[Char6(Fe_3O_2)]}, and {x[Char6(Fe_5O_2)]} where x = 2–12; XPS data of char samples containing iron, obtained from catalytic steam gasification experiments, identified iron oxide and an increase in organic oxygen, and XRD identified Fe_2O_3 as the major iron phase.

Calculations of the concentration of water molecules for the char surface obtained from MOPAC, and the rate of water molecules impacting on the char surface, indicate a high rate of water molecules impacting on the char surface. H_2O was shown to be weakly physically adsorbed onto the char surface (−2 to −6 kcal/H_2O), and strongly chemi-adsorbed on active sites by forming the coordination bond [H_2O→ Fe] on [Fe–C] sites. The changes in ΔH_f for water sticking on the various char models cover a wider range of values (−15 to −80 kcal/H_2O) because of the various orientations of the [Fe–C] groups; for some of these sites access to the iron centre appeared to be hindered. Systematic studies of molecular models containing a number of [Fe–C] sites provided energy changes for each of the various configurations; while a full discussion of the details of this modelling effort is outside the scope of the present paper, the energy for chemi-sorption of water on the Fe centre varied considerably, especially when water molecules also formed coordination bonds to available [Fe–O]

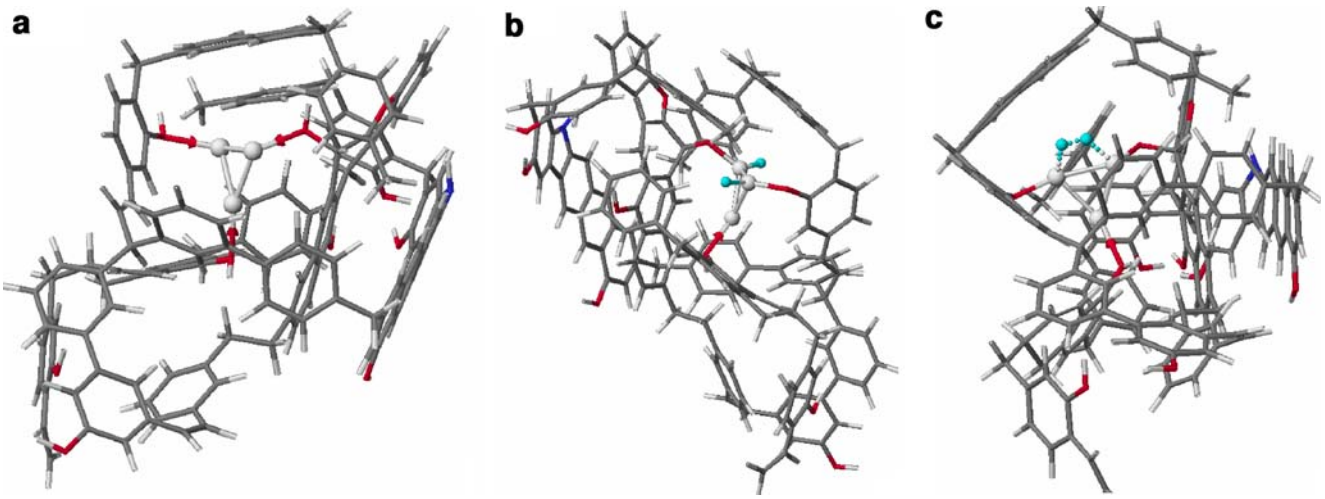

Fig. 3a–c [Char6(Ni_3)] (Ni = ◯, O = red) structures used for 1scf-DFT computations of H_2 formation. **a** Initial model, **b** H(●) abstracted from OH, **c** H–H (●) on Ni_3 prior to loss as H_2

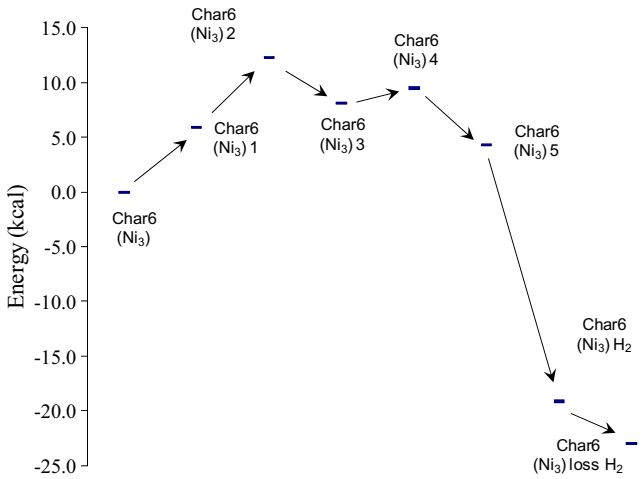

Fig. 4 1scf-DFT energy changes for H_2 abstraction from Char6(Ni_3)

groups. For example, 1scf-PM5 results for {3[Char6(Fe_3) 3(H_2O)]} gave a difference in ΔH_f of −60 kcal for chemi-adsorption of the water molecules on the [Fe–O] groups, but for {4[Char6(Fe_3) 4(H_2O)]}, in which all water molecules were coordinated to [Fe–O] sites, the difference was only −8 kcal. The coordination of H_2O to the [Fe–C] site in the model {2[Char6(Fe–C)$_2$(Fe ←OH)(H_2O)]}, in which H_2O was situated at two different [Fe–C] sites, gave −27 kcal for one site and −16 kcal for the other. Data was also obtained for the models {2[Char6]}, {2[Char6 2(H_2O)]}, {2[Char6(Fe_3)]} and {2[Char6(Fe_3) 2(H_2O)]}, in which water molecules were either physically adsorbed onto the char, or chemi-adsorbed onto either the [Fe-C] site or the [Fe-O] site; this work is continuing with char models containing a greater variety of clusters.

The modelling also examined the impact of larger iron oxide particles; large metal oxide particles would not impart catalytic activity, but would cause changes to the char surface area. The impact of the size of a metal particle on the char surface is shown by the results for the model {12[Char6(Fe_3)](Fe_{12})]}; [Fe_{12}] was added as a particle in the centre of the large char molecular model, and this resulted in the formation of a micro-pore 2 nm in diameter at the surface of the char model. The size of the [Fe_{12}] was about 0.5 nm, and the char model about 6 nm. This example illustrates the complicated nature of catalytic steam gasification, as accessibility of steam to active sites would depend to a large extent on the char surface area, and the char morphology could be changed significantly by pores formed as a result of large-sized metal oxide particles within char.

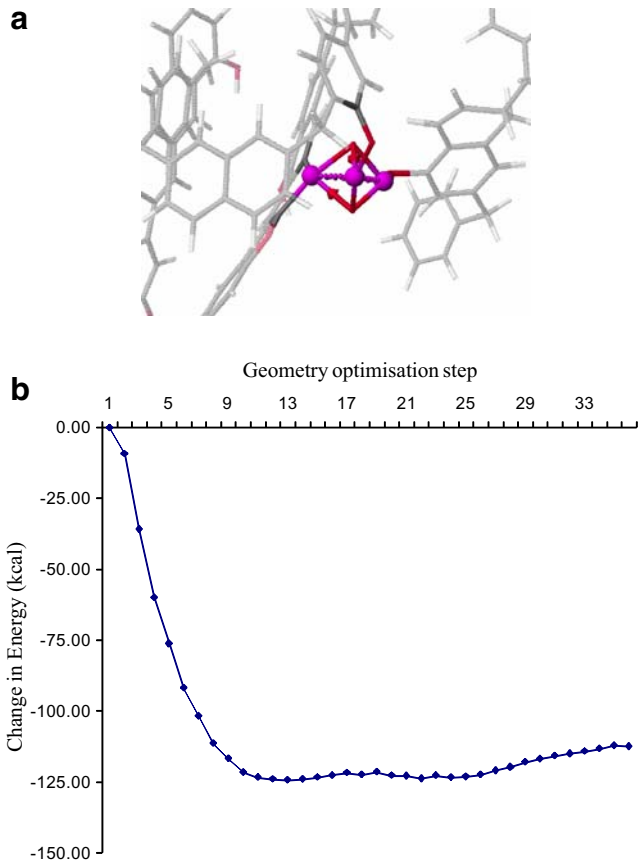

Fig. 5a,b DFT results for Char6(Fe_3O_2) (after loss of CO and H_2). **a** Optimised structure (● Fe), **b** change in energy with each optimisation step

Discussion

Molecular model of low-rank coal

Two molecular models of low-rank coal were initially examined: one based on data from 'woody' samples of coal, and the other on average, or typical, properties of brown coal as shown in Table 1. The primary objective was to construct a model of low-rank coal that encompassed measured properties, and provided the spatial distribution of oxygen functional groups in the 3D molecular structure required for octahedral and tetrahedral transition metal complexes [16]. The size of the molecular model was restricted to the limits imposed by computer resources. It was found that the spatial distribution of the carboxyl and hydroxyl groups of a moderately sized 'woody' model was not suitable for octahedral metal complexes. This difficulty could be remedied in part by stacking a number of semi-helical structures together randomly, so that carboxyl and phenolic groups were available in various orientations; however, the resulting molecule did not encapsulate the major experimental properties of low-rank coals and was too large for SE computations. Consequently, further work on models based on woody coal samples was not pursued. The model discussed here has proved useful in experimental studies of metal mediated chemistry during pyrolysis and catalytic gasification, especially in modelling the transformations of inorganic complexes in coal, into char with metal species observed during

pyrolysis reactions and steam gasification; this molecular model is nonetheless a simplified molecular representation of low-rank coal.

The bond lengths and angles observed in the SE-optimised molecular model were typical for aliphatic, aromatic, and oxygen functional groups. The optimised model with water exemplifies the hydrophilic properties of low-rank coals. i.e. atomic partial charges were: oxygen groups − 0.38 to − 0.51; carboxyl hydrogen, +0.33 to +0.35, phenolic hydrogen +0.28 to +0.32, and carboxyl carbon, +0.48 to +0.44. Extensive hydrogen bonding was observed, and this was enhanced when water molecules and aqua-ionic species were added to the structure. For example, O···H distances between water and carboxyl groups were: 2.01 Å (H_2O)···(HOOC−); 2.24 Å, with phenolic groups (OH)···(HOOC−), and 2.56 Å (OH)···(OH). The extensive network of hydrogen bonds with coal functional groups contributed an additional −1.1 kcal per water molecule to the calculated ΔH_f of the structure. This result is consistent with the experimental observations for brown coal, in which between 10 wt% and 20 wt% of moisture is hydrogen bonded within the coal matrix and contributes significantly to the lower energy conformation of the molecule. The data also shows a difference of −3.4 kcal per water molecule between coal containing water and water vapour (non-hydrogen bonded water molecules). The ΔH_f for the SE-optimised coal molecular model yielded a linear relationship with the number of water molecules in coal, as shown in Fig. 6.

Brown coal is mined with ~60 wt% of water; these large amounts of water could be modelled by placing the bulk of the water molecules in spaces between the coal molecules. Experimental data shows that most of the water in mined coal behaves as bulk, or liquid, water and the coal volume expands to accommodate the large amount of water, and shrinks when the water is removed. The molecular volume

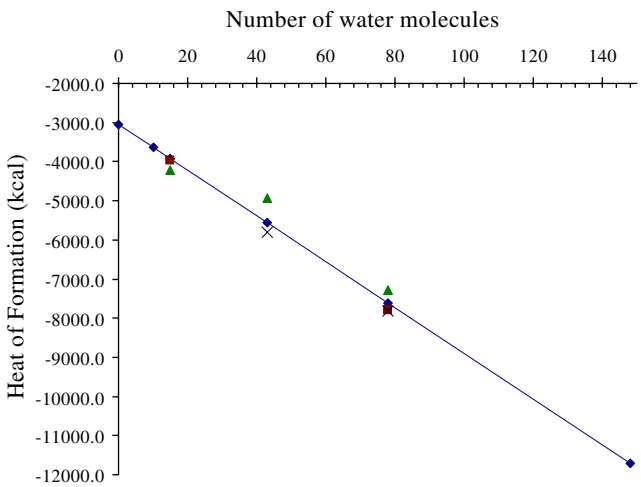

Fig. 6 Heat of formation (SE) for coal with water (♦); coal with water and Na^+(■); Ca^{2+} (▲); Na^+, NaCl (X)

was relatively constant when water molecules were situated within the macromolecular structure (up to 20 wt% water), but the calculated volume increased significantly with >50 wt% water, indicating a lower density, as observed for mined coal; the calculated density of the 2D coal fragment (used to construct the 3D structure) was 1.46 g cm^{-3}, which is comparable to the value 1.44 to 1.52 g cm^{-3} reported for dry brown coal [29].

Figure 6 also shows the ΔH_f values for coal molecular models containing the same number of water molecules and sodium, or calcium, or sodium and sodium chloride (the latter is similar to Na^+ and NaCl found in brown coal). The water molecules exert the major impact on the stability of the coal molecule; coal with ionic Na^+ and carboxylate, surrounded by water molecules and hydroxyl groups, formed energetically favoured structures, due to the strength of the ionic bond [$COO^-\cdots Na^+$] and close proximity of water and coal functional groups to Na^+. The optimised coal molecular models also contained cations, which formed shorter hydrogen bonds; for example, in the structure with Na^+, the carboxylate cation shared the adjacent carboxyl hydrogen. The nearest neighbour groups to sodium in this structure were six oxygen groups at ~2.5 Å: two H_2O, one carboxylate, and three hydroxyl. The atomic partial charge on sodium was +0.4, and on the two oxygen atoms of the carboxylate anion > −0.5. Coal molecular models with water, and Na^+ and Cl^-, were optimised with the ions separated by water molecules within the coal molecule, effectively replacing the hydrated sphere. In practice, most of the NaCl can be washed out with water from brown coal. Mildly acidic conditions are required to remove cations such as Na^+, Mg^{2+} and Ca^{2+}.

The coal model with Ca^{2+} formed a less energetically favoured structure compared to the same coal model containing an identical number of water molecules. This result was due mainly to the size of Ca^{2+}, which cannot fit as easily as Na^+ in spaces near the carboxylate anions. Formation of H_3O^+ from the carboxyl groups in coal was energetically favoured; these results are consistent with experimental data in which acid base reactions are associated with the addition of calcium to brown coals, e.g.

$$Ca(OH)_2 + \{Coal(COO^-)_2\ 2H_3O^+ \rightarrow \{Coal(COO^-)_2\ [Ca^{2+}]\} + 4H_2O$$

Models of coal with Ca^{2+} included a ground state in which the cation was surrounded by five H_2O molecules (Ca ←OH_2 distances 2.27 Å, 2.36 Å, 2.29 Å) and hydroxyl group (Ca←OH at 2.72 Å); one monodentate carboxylate (Ca···O 2.28 Å) and the other bidentate (Ca···O 2.42 Å and 2.69 Å). Partial charges on oxygen were: carboxylate −0.7 to −0.5; water −0.45; phenolic −0.44; calcium +0.6. In the coal model with 43 water molecules, calcium was

surrounded by water and coal functional groups at a considerable distance from the carboxylate anions; the two coal carboxylate groups were involved in strong hydrogen bonding with two water molecules and two hydroxyl groups. Energetically favoured structures with calcium were obtained with the cation placed in the space between two coal molecules and two adjacent carboxylate groups (intermolecular ionic-bonds), and a large number of water molecules between the coal molecules; the increased stability was due to the additional space available for the calcium ion.

Transition metal complexes

Molecular models of low-rank coals containing transition metal complexes must encompass the chemistry of aqua-transition metal complexes. Brown coal containing varying amounts of transition metal complexes has been prepared by mixing the coal with a solution of the salt and adjusting the pH of the mixture (it is necessary to avoid formation of metal hydroxide precipitates during this procedure). The addition of Fe(III) and Co(II) to brown coal has been discussed [19, 20, 30]. The amount of metal complex added to coal by simply mixing with coal was <1 wt% on a dry coal weight basis; this is similar to the amount added as aqua mono-nuclear metal complexes in the coal molecular models (Table 2). At pH 2.5 the bulk of the species in solution are the octahedral aqua complexes $[M(H_2O)_6]^{n+}$ (n=2 or 3, M=Cr, Fe, Co, Ni), and at pH values between 3 and 5, multi-nuclear aqua complexes formed in solution [39]. The general chemistry for adding aqua mono-nuclear metal species to brown coal may be written as (n=2 or 3):

$$\{\mathrm{Coal(COOH)_n}\} + \left[\mathrm{M(H_2O)_6}\right]^{n+} \rightleftarrows \left\{\mathrm{Coal(COO)_n}\left[\mathrm{M(H_2O)_{(6-n)}}\right]\right\} + \mathrm{nH_3O^+}$$

The chemistry for multi-nuclear metal complexes is illustrated by the iron complex:

$$\{\mathrm{Coal(COOH)_4}\} + \left[\mathrm{Fe_2(OH)_2 8H_2O}\right]^{4+} \rightleftarrows \mathrm{Coal}\left\{\mathrm{(COO^-)_4 Fe_2(OH)_2 4H_2O}\right]^{4+}\right\} + 4\mathrm{H_3O^+}$$

The amount of metal added to coal would be determined by the amount of $[OH]^-$ used to adjust the pH of the mixture, because this would drive the reaction to completion by removing the $[H_3O]^+$ released from the coal. The nature of the metal complex added to the coal molecule, however, would also depend on the solution chemistry, in which further addition of $[OH]^-$ to increase the pH would form multi-nuclear transition metal complexes.

The octahedral metal complexes in coal were bonded to mono-dentate carboxyl groups; these also formed hydrogen bonds between coordinated water molecules and other water molecules, and with hydroxyl groups. Two examples for the $[Ni(H_2O)_4]^{2+}$ octahedral complex illustrate this point; these were similar configurations, with the exception that the second model included a formal hydrogen bond between the carboxyl groups bonded to nickel and water molecules in the proximity of the transition metal species. The 1scf result for the first configuration was of a distorted nickel structure with one carboxyl group acting as a bi-dentate; the second model provided a slightly more stable and undistorted octahedral nickel structure, which contained a number of hydrogen bonds involving the coordinated ligands, as shown in Fig. 7.

Table 2 lists data for the coal model containing transition metal complexes; 1scf computations of coal containing octahedral metal complexes gave bond lengths and angles typical for these transition metals [16, 17]. 1scf-MECI computations for mono-nuclear complexes provided singlets for Cr(II), Fe(II), Ni(II), and doublets for Cr(III), Co (II) and Fe(III) calculated at −1.2 eV to −2.5 eV lower energy. The ΔH_f values (Fig. 8) show that all coal models containing mono-nuclear metal complexes, except that for the model containing Co(II), were similar to that for [Coal $(43H_2O)$], indicating the water in coal exerted a major influence on the energy of these molecular models. The atomic partial charges (Table 2) on the metal centres for the coal models were lower for Cr and Ni, and higher for Fe and Co. The atomic partial charge on the Cr(II) complex was unusually low at −0.6 (SE-optimised structure) and this is likely to be due to the shorter coordination bonds lengths (Cr ←OH_2 and Cr ←OH, 1.99 Å and 2.00 Å) and higher bond orders (0.6 to 0.7) in this structure because of increased electron density donated by the lone pair to the

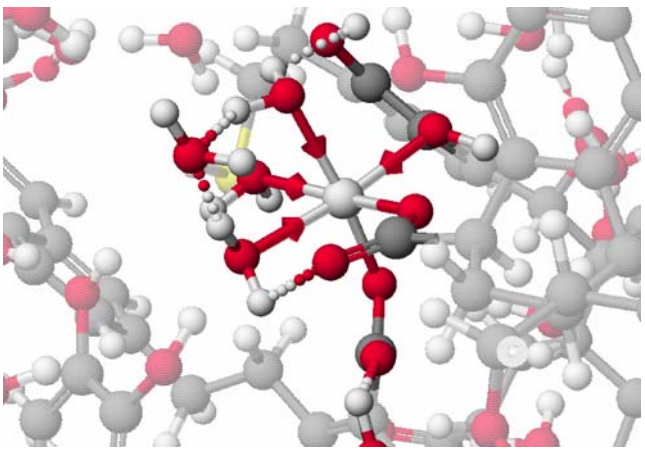

Fig. 7 Nickel complex bonded to carboxylate and coordinated water molecules, with hydrogen bonds (Ni = , O = , H = , C = , H bonds)

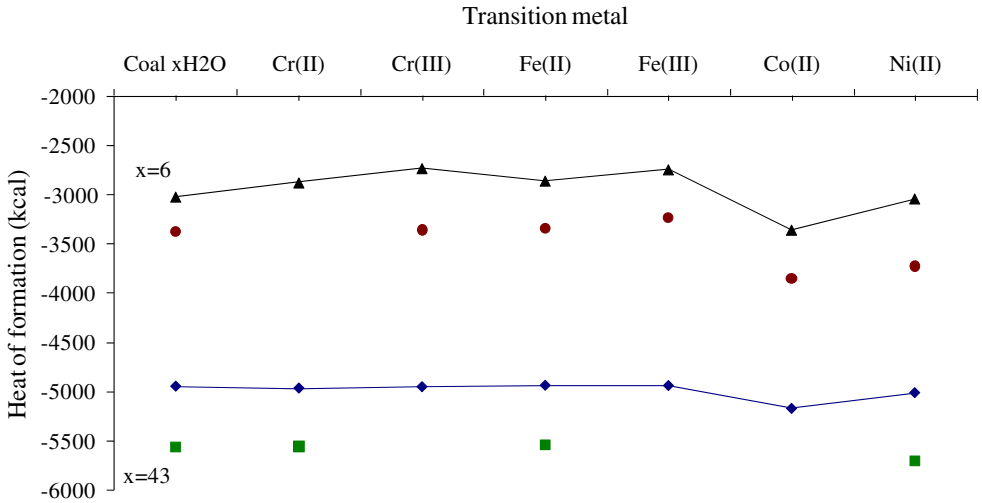

Fig. 8 Heats of formation for coal and transition metal complexes: {coal[M] $43H_2O$} (◆1scf, ■SE) and {coal $[M_2(OH)_2(H_2O)_4]$} (▲1scf, ●SE)

metal. The oxygen on ligands coordinated to Cr(II) also contained a lower partial charge (−0.2 to −0.3) and the hydrogen higher partial charges (0.3 to 0.4) compared with those in the original coal molecular model. The 1scf computation, on the other hand, provided a typical Cr(II) complex, with a partial charge of almost zero, and typical Cr–O bond length (1.95 Å) and bond order (0.7), coordination bond lengths (2.15 Å and 2.17 Å) and bond orders (0.4).

1scf and SE ΔH_f values for coal with mono-nuclear and the di-nuclear complexes are plotted in Fig. 8. The models with the μ-hydroxyl poly-nuclear complex contain H_2O and OH equivalent to $6H_2O$, and thus have been compared with the ΔH_f value of the coal molecular model with $6H_2O$. The variations in ΔH_f with transition metals were higher by 5% to 10%, except for cobalt, which was lower by −11% (compared with the coal model with the equivalent number of water molecules). 1scf-MECI computation for the di-nuclear complexes provided the following lower energy levels: Co(II) singlet −0.01 eV, Cr(III) triplet −1.15 eV, and Fe(III) triplet −2.26 eV. Generally, the energy of the coal model containing transition metal structures was stabilised by the formation of [M–O] and coordination [M ←OH] bonds; however, the molecular structure was destabilised by the larger size of the octahedral complex, which imposed steric strain on the macromolecule and disrupted the hydrogen bonding between water molecules and oxygen functional groups. 1scf provided regular octahedral complexes, while the SE-optimised structures were often distorted, because of the increased formation of hydrogen bonds. SE results obtained for Fe(II) and Ni(II) complexes show the iron complex ground state was similar in energy to that of the coal model, but the distorted nickel complex was calculated with a lower energy by −10.5% compared with [Coal ($6H_2O$)].

Coal molecular models with a greater amount of iron (5.4 wt% and 6.5 wt% iron in coal) were created by using the $[Fe_3(OH)_n]^{(9-n)+}$, and $[Fe_4(OH)_n]^{(12-n)+}$ multi-nuclear complexes; these models were less energetically favoured compared with the same coal structure containing an equivalent number of water molecules. Such molecules could form relatively stable structures, however, if additional water molecules were incorporated by the iron complexes within the coal model. Stable structures were also obtained by placing the large multi-nuclear complexes in spaces between two or more coal molecular models. The latter arrangements were particularly favoured in coal molecules containing large amounts of water. These data further emphasise the importance of steric factors on the stability of low-rank coals containing transition metal complexes, and reinforce the notion that these large poly-nuclear hydroxyl complexes would be situated in regions of the coal macromolecule with space to accommodate them, such as spaces between the macromolecules, which also accommodate large amounts of water.

Formation of char with metal oxides

Pyrolysis chemistry of low-rank coal, particularly at low temperatures, is dominated by decomposition of oxygen functional groups into CO_2 and CO [19–21]. Metal aqua-hydroxyl complexes in coal are transformed into metal oxides on heating; as the temperature is increased they form lower oxidation states and ultimately metallic phases in char. Modelling with coal containing poly-nuclear hydroxyl iron species, for example, involves carboxyl groups decomposing into CO_2 and CO, and poly-nuclear iron hydroxyl complexes transformed into Fe(III) carbonates that decompose into oxides; with increasing temperature these form Fe(II)Fe(III) oxides, further reduction ultimately forming metallic iron. Pyrolysis chemistry may occur by a number of reaction routes, but the major route has been shown to involve the formation of metal carbonates and radical species [20, 21]. Two examples of molecular models of char are shown in

Fig. 9; char with Fe_3O_4 (Fig. 9a) resembles the elemental composition and iron oxide phases observed in char samples obtained when coal containing iron hydroxyl species was heated at 400–600 °C under nitrogen; char with the Fe_3 cluster (Fig. 9b) is used to model metallic Fe phases observed in char prepared at >700°C. The comparison is reasonable between experimental weight loss and calculated data for char models, shown in Table 3; a higher ratio of CO_2:CO was measured for coal containing iron complexes, consistent with the iron carbonate mechanism. Experimental data for the pyrolysis of brown coal containing cobalt species was similar to that obtained for coal containing iron species [32]. Pyrolysis at higher temperatures yielded a gaseous mixture of H_2, CO_2, CO, and CH_4; the mechanism for the formation of H_2 and CO from the pyrolysis of brown coal char containing Fe, at elevated temperatures, has been discussed [21, 22].

The 1scf ΔH_f values for {Char6 [M_3O_n]} (M=Cr, Fe, Co, Ni) are plotted in Fig. 10; these decrease with an increase in oxygen (n=0 to 3), indicating that the stability of these complexes in coal follows the trend Fe <Cr <Co < Ni. Data on the structure of each cluster used in these models, and that found in the literature, was comparable to our SE and DFT results [21, 22, 33–40]. SE computations for these char models always yielded structures of lower energy when hydrogen was abstracted by the metal cluster from nearby OH and CH groups to form [M–H], [M–O] and [M–C] bonds. Char containing Co clusters usually favoured [Co–O] and [Co–H] bonds, with closer proximity to carbons to form weak [Co–C] bonds. The SE results for [Ni_3O_n] show that as (n) decreased from 3 to 0, increasing interactions occurred between Ni centres and π electrons of nearby phenyl groups. The geometry of optimised char models containing [Ni_3] clusters also changed as the amount of oxygen in the cluster decreased; the partial charges on Ni decreased from 0 to −0.8, consistent with increased donation of electron density from delocalized π electrons to the metal centres. The cluster in {Char6[Ni_3]} was optimised with a linear geometry in which the Ni atoms have formed the maximum number of [Ni ←OH] coordination bonds, and maximised the interactions of each Ni with π electrons in phenyl groups. The [Ni-O] bond orders also decreased with decreasing oxygen in the cluster, while the [Ni-C] bond orders increased; i.e. bond orders for [Ni_3O_2]: Ni–O=1.0–0.9; Ni–C=0.3. Bond orders for [Ni_3O]: Ni–O=0.5–0.9; Ni–C=0.8–0.6. Bond orders for [Ni_3]: Ni–O= 0.2; Ni–—=0.8, 0.3.

Mechanisms of H_2 and CO formation and catalytic steam gasification

SE computations have been carried out on molecular structures postulated for reaction routes leading to the formation of the gases CO_2, CO, and H_2. The SE results have shown that hydrogen abstraction with the formation of [M–H] and [M–C] bonds was energetically favoured; consequently, a reaction route for H_2 formation has been modelled. 1scf-SE and 1scf-DFT computations have been particularly useful in these studies, and some results are shown in Figs. 3 and 4; the structures shown in Fig. 3b and c correspond to Char6 (Ni_3) 2 and Char6(Ni_3) 5 in Fig. 4. The mechanism of H_2 formation by hydrogen abstraction has been shown to be plausible for all of the clusters discussed. Detailed modelling for the formation of CO was complicated, however, by data that indicated a concerted mechanism was energetically favoured, and this included structures with [M–H] bonds formed by hydrogen abstraction. Other reaction routes also need to be considered, including the formation of π complexes {for example [(π)Ni..(Ph)]} and the formation of Co and Ni carbonyl clusters. Further complications in these reaction routes include post-gasification reactions between CO with H_2O ($CO + H_2O \rightarrow CO_2 + H_2$), reduction of metal oxides by CO, and reaction between nCO and [M_m] to form the transition metal carbonyls [$M_m(CO)_n$].

The mechanisms we have postulated to date have been based on changes in the ΔH_f values calculated for each molecular structure used to describe the particular reaction route. Loss of CO_2 via the iron carbonate intermediate, and transfer of hydrogen from the hydroxyl ligand to the carbon centre leads to iron oxides, illustrated in Fig. 9a; loss of CO and H_2 is accompanied with the formation of metallic iron,

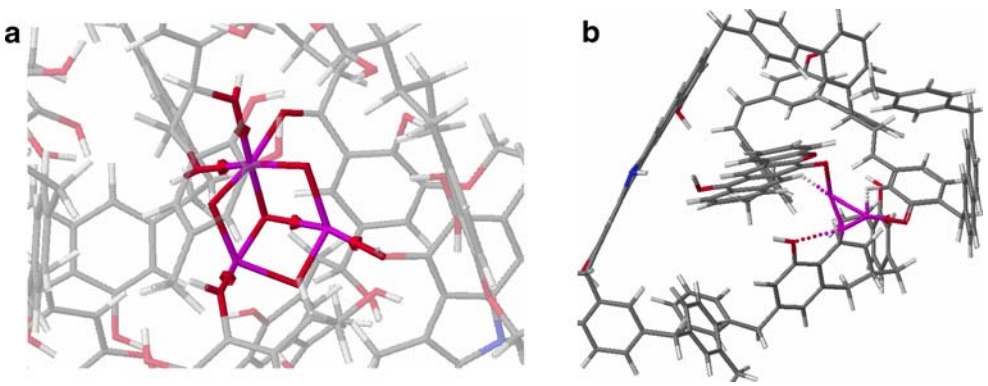

Fig. 9 Structures of **a** [Fe_3O_4] in Char1 and **b** [Fe_3] in Char6

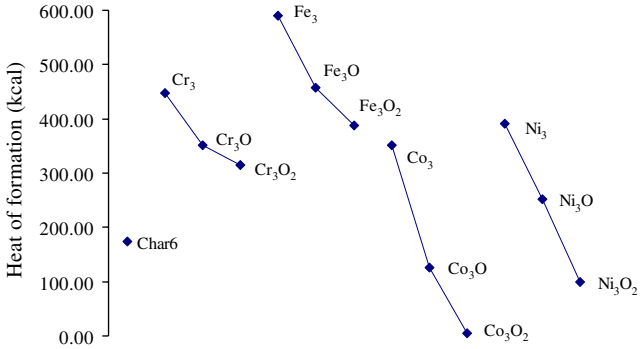

Fig. 10 Heat of formation for Char6 containing metal clusters

illustrated by the model in Fig. 9b. The reduction of iron oxides during pyrolysis occurs in stages, from Fe_2O_3 to Fe_3O_4 at lower temperatures and metallic iron (modeled as the Fe_3 cluster) at higher temperatures. The short Fe···H distances shown in Fig. 9b, also illustrate the structure that forms prior to hydrogen abstraction. The modelling results agree with experimental data, including weight loss, yields of gases, identification of iron carbonate (XPS) and the various phases of iron oxide and metallic iron (XRD).

The structures developed for char formation with transition metal clusters were used to identify the active site for catalytic steam gasification chemistry; the modelling studies also predicted the formation of iron oxide phases during steam gasification (XRD), the increase in inorganic oxygen (iron oxide phase) and increase in organic oxygen (added to char) observed experimentally using XPS. The mechanistic insights for catalytic steam gasification (following the formation of the [Fe–C] site) provided by modelling computations can be illustrated by the simplified scheme:

A Chemi-adsorption of H_2O: {char[Fe–C]} + H_2O → {char[C–Fe ←OH_2]}
B Hydrogen abstraction: {char[C(OH)Fe..H]}
C Hydrogen transfer, oxygen insertion: {char[C–O–Fe]..(H_2)}
D Loss of hydrogen: {char[C–O–Fe]..(H_2)} → {char[C–O–Fe]} + H_2
E Formation of CO: {char[C–O–Fe]} → {char[–Fe..(CO)]}
F Loss of CO and new [Fe–C] site: {char[–Fe..(CO)]} → {char[C–Fe]} + CO

Our mechanism identifies the central aspect of catalytic steam gasification as the chemi-adsorption of H_2O on the active sites [M–C]. The [Fe–C] site has significant ionic character; e.g. in [Char(Fe_{3B})] atomic partial charges (SE-PM5) were: Fe=+0.5 to + 0.9; ionic attraction between the $\left[Fe^{\delta+}(-C)\right]$ group and the negative charge on $\left[O^{\delta-}-H_2\right]$ would favour the formation of the [H_2O→Fe-C] complex. Modelling of the chemi-adsorption of H_2O on active sites also addressed the accessibility of these active sites to steam molecules, which depends primarily on the stereochemistry of the molecular model. This was modelled using larger molecules containing a number of [Fe–C] sites and the results show a variety of ΔH_f values resulting from the coordination of a water molecule to the iron centre, because of the different configurations about the various [Fe_3] clusters. The energetically favoured result was obtained for the most accessible [Fe–C] group; concerted chemistry, which involved the formation of [Fe–H] and [H_2O→ Fe–C] bonds, provided the most energetically favoured structure. For example, a char model that contained the [Fe–H] bond (hydrogen abstraction from C–H) and formed the [C–Fe ←OH_2] coordination bond with water, provided a ΔH_f value −80 kcal lower than the same model with the water molecule at a large distance. SE modelling results also show a number of H_2O molecules may chemi-adsorb onto the active sites of the large structures with concurrent physical adsorption of H_2O molecules on the char surface. Each of these structures has different ΔH_f values; physical adsorption of water molecules on char generally contributed −2 kcal to −6 kcal to the enhanced stability of the structure, while chemi-adsorption of H_2O on [Fe–C] contributed between −20 kcal and −80 kcal. The great variation in orientation of [Fe–C] and [Fe–O] groups observed in large char molecular models, and a combination of various clusters in char, yields a wide range of changes in ΔH_f values for water molecules coordinated to iron centres; this range of values increased for char models containing clusters of Cr, Co, and Ni.

A full treatment of the dynamics of heterogeneous catalysis is required to relate the rate with which gas molecules stick to the active sites on the char surface with the chemical kinetics that convert the mobile chemicals at the surface into product(s) that are transported away. This requires a dynamic treatment of each individual reaction step for the molecular transformations and is beyond the scope of the present discussion. In practice, catalytic gasification at 800–900°C would be controlled by the intrinsic chemical kinetics of the system. The water molecules impact on the char surface at a high rate per unit time, and the overall rate of gasification would be related to the number of accessible active sites, and the energy changes when water molecules stick to these active centres. The presence of non-catalytic, large metal-oxide species within the char would increase the char porosity and this in turn would improve the accessibility of active sites to water molecules. The catalytic mechanism must include the reformation of active sites; as char is consumed, the relative concentration of the metal oxide species increases. This may lead to an increase in the number of accessible sites and, in turn, increase the rate of gasification. But if the metal oxide agglomerates into large particles, catalytic activity may decrease; large amounts of metal oxide particles on the char surface would impact on the

porosity of these particles. Practical considerations of catalytic steam gasification would include reaction by a mixture of O_2/H_2O with coal, to generate heat from the exothermic reaction ($2C + O_2 \rightarrow 2CO$). In this case, the molecular modelling effort would include reactions of O_2 in parallel with steam gasification, which would be determined largely by the relative concentrations of O_2 and H_2O.

Computations of molecular models of char containing transition metal clusters are continuing, as part of our effort to develop catalysts for steam gasification of low-rank coals. The complicated systems studied and the very large computer resources needed for these calculations prevent rigorous treatments of the reaction mechanisms; simpler molecular modelling schemes that may enable us to rigorously examine specific steps in the reaction mechanisms are currently being considered.

Summary

We have developed a molecular model of low-rank coal that has encapsulated the measured properties of brown coal; this structure has modelled hydrogen bonded water, retention of bulk water, and the nature of ionically bonded aqua-inorganic species. The coal structure has also modelled aqua-transition metal mono- and multi-nuclear hydroxyl species as octahedral complexes forming bonds with carboxyl groups and coordination bonds with hydroxyl groups.

The molecular model of coal has been used to develop char molecular models, mimicking pyrolysis chemistry; the modelling data has compared well with experimental data for brown coal. These modelling studies of pyrolysis chemistry have also included the transformations of coal containing metal complexes into char containing metal oxides and metallic phases observed for brown coal samples over the temperature range 250 °C to 800 °C. Models of char containing metal clusters were optimised using SE and DFT techniques, and these models were used to study the reaction routes for H_2 and CO formation. The char models were effective for studies of pyrolysis reaction routes, identifying the [Fe–C] groups as the active site for iron-catalysed steam gasification. Our modelling of catalytic steam gasification has demonstrated that chemi-adsorption of water molecules to the [Fe–C] centres is a critical step in steam gasification, and has enabled mechanistic studies of catalytic steam gasification, which included reaction routes for hydrogen abstraction and oxygen insertion to H_2 and CO formation. Modelling data was consistent with experimental data obtained for pyrolysis and steam gasification of brown coal containing iron species.

Acknowledgements This work was supported by grants and computer facilities from VPAC, and the provision of computer time by APAC-NF under the Merit Allocation Scheme. Rheinbraun GBT supplied samples of German brown coal and Loy Yang Open Cut Mine supplied samples of Victorian brown coal. Experimental data were provided by M. Roarun, Dr. R. Glaisher and L. Del Papa.

References

1. Stout SA, Boon JJ, Spackman W (1988) Geochim Cosmochim Acta 52:405
2. Levine JR (1993) AAPG Stud Geol 38:39–77
3. Shevchenko SM, Bailey GW (1996) Crit Rev Environ Sci Technol 26:95–153
4. Shinn JH (1984) Fuel 63:1187–1196
5. Carlson GA, Granoff B (1991) Coal Sci II ACS 159–170
6. Nakamura K, Takanohashi T, Iino M, Kumagai H, Sato M, Yokoyama S, Sanada Y (1995) Energy Fuels 9:1003–1010
7. Takanohashi T, Kawashima H (2002) Energy Fuels 16:379–387
8. Mathews JP, Hatcher PG, Scaroni AW (2001) Energy Fuels 15:863–873
9. Derbyshire F, Marzec A, Schulten H-R, Wilson MA, Davis A, Tekely P, Delpuech J-J, Jurkiewicz A, Bronnimann CE, Wind RA, Maciel GE, Narayan R, Bartle K, Snape C (1989) Fuel 68:1091–1106
10. Faulon J-L, Carlson GA, Hatcher PG (1994) Org Geochem 21:1169
11. Hatcher PG, Lerch HE III, Koytra RK, Verheyen TV (1988) Fuel 67:1069
12. Hatcher PG, Clifford DJ (1997) Org Geochem 27:251
13. Hatcher PG (1989) Org Geochem 16:959–968
14. Hüttinger KJ, Michenfelder AW (1987) Fuel 66:1164
15. Drobniak A, Mastalerz M (2006) Int J Coal Geology 66:157–178
16. Domazetis G, James BD (2006) Org Geochem 37:244–259
17. Domazetis G, Liesegang J, James BD (2005) Fuel Process Technol 86:463–486
18. Verheyen TV, Perry GJ (1991) In: Durie RA (ed) The science of Victorian brown coal. Butterworth Heinemann, Oxford
19. Domazetis G, Raoarun M, James BD (2005) Energy Fuels 19:1047–1055
20. Domazetis G, Raoarun M, James BD (2006) Energy Fuels 20:1997–2007
21. Domazetis G, Raoarun M, James BD (2007) Energy Fuels 21:2531–2542
22. Domazetis G, Raoarun M, James BD, Liesegang J (2008) General Catalysis A 340:105–118
23. ACD/ChemSketch Freeware, version 10.00 (2006) Advanced Chemistry Development, Inc., Toronto, ON, Canada, www.acdlabs.com
24. CAChe ab initio version 5.04 (2000–2002) Fujitsu Ltd
25. Stewart, JJP, "MOPAC 2002", Fujitsu Limited, Tokyo, Japan
26. Jaguar, version 6.5 (2005) Schrödinger. LLC, New York, NY
27. Domazetis G, Raoarun M, James BD, Liesegang J, Pigram PJ, Brack N, Glaisher R (2006) Energy Fuels 20:1556–1564
28. Murata S, Hosokawa M, Kidena K, Nomura M (2000) Fuel Process Technol 67:231–243
29. Yost RS, Creasy DE (1990) Fuel 69:648–650
30. Arvizu GL, Calaminici P (2007) J Chem Phys 126:194102–10
31. Liu F, Zhang X-G, Liyanage R, Armentrout PB (2004) J Chem Phys 121:10976–15
32. Del Papa L (2007) Honours Thesis, Department of Chemistry, La Trobe University
33. Diéguez O, Alemany MMG, Rey C, Ordejón P, Gallego LJ (2001) Phys Rev B 63:2005407–6
34. Noya EG, Longo RC, Gallego LJ (2003) J Chem Phys 119:11130–11134

35. Gutsev GL, Khanna SN, Rao BK, Jena P (1999) J Phys Chem A 103:5812–5822
36. Liu F, Zhang X-G, Liyanage R, Armentrout PB (2004) J Chem Phys 121:10976–10990
37. Schimmel PHA, Ruttink PJA, de Jong BHWS (1999) J Phys Chem B 103:10506–10516
38. Temelso B, Sherrill CD, Merkle RCM, Freitas RA Jr (2006) J Phys Chem A 110:11160–11173
39. Gutsev GL, Mochena MD, Bauschlicher Jr CW (2004) J Phys Chem A 108:11409–11418
40. Greenwood NN, A Earnshaw (1997) Chemistry of the elements. 2nd edn. Butterworth, Heinemann, Oxford